Specific removal of TACC3–ch-TOG–clathrin at metaphase deregulates kinetochore fiber tension

Liam P. Cheeseman[1], Edward F. Harry[2,3], Andrew D. McAinsh[2], Ian A. Prior[1] and Stephen J. Royle[1,2,*]

[1]Department of Cellular and Molecular Physiology, Institute of Translational Medicine, University of Liverpool, Crown Street, Liverpool L69 3BX, UK
[2]Centre for Mechanochemical Cell Biology, Division of Biomedical Cell Biology, Warwick Medical School, University of Warwick, Gibbet Hill Road, Coventry CV4 7AL, UK
[3]Molecular Organization and Assembly in Cells Doctoral Training Centre, University of Warwick, Coventry CV4 7AL, UK
*Author for correspondence (s.j.royle@warwick.ac.uk)

Accepted 1 February 2013
Journal of Cell Science 126, 2102–2113

doi: 10.1242/jcs.124834

Summary

Microtubule-associated proteins of the mitotic spindle are thought to be important for the initial assembly and the maintenance of spindle structure and function. However, distinguishing assembly and maintenance roles for a given protein is difficult. Most experimental methods for protein inactivation are slow and therefore affect both assembly and maintenance. Here, we have used 'knocksideways' to rapidly (~5 minutes) and specifically remove TACC3–ch-TOG–clathrin non-motor complexes from kinetochore fibers (K-fibers). This method allows the complex to be inactivated at defined stages of mitosis. Removal of TACC3–ch-TOG–clathrin after nuclear envelope breakdown caused severe delays in chromosome alignment. Inactivation at metaphase, following a normal prometaphase, significantly delayed progression to anaphase. In these cells, K-fiber tension was reduced and the spindle checkpoint was not satisfied. Surprisingly, there was no significant loss of K-fiber microtubules, even after prolonged removal. TACC3–ch-TOG–clathrin removal during metaphase also resulted in a decrease in spindle length and significant alteration in kinetochore dynamics. Our results indicate that TACC3–ch-TOG–clathrin complexes are important for the maintenance of spindle structure and function as well as for initial spindle assembly.

Key words: Checkpoint, Knocksideways, Microtubule, Mitotic spindle, Rapid inactivation

Introduction

Accurate chromosome segregation by the mitotic spindle is essential for life. It must proceed error-free in order to prevent cell death, cancer or birth defects (Murray, 2011). The spindle apparatus is an ensemble of microtubules (MTs), motors and non-motor proteins (Peterman and Scholey, 2009). Non-motor spindle proteins are involved in the initial assembly of the spindle and the maintenance of spindle structure and function. However, distinguishing the role in assembly and maintenance for a given spindle protein is problematic.

Over the last decade, RNA interference (RNAi) has dominated cell biology and it is the method of choice for understanding the function of spindle proteins. However, interpreting depletion phenotypes at later stages of mitosis is problematic because any defects observed could be due to errors that occurred at earlier stages, e.g. assembly of a defective spindle. In this study, we have used the 'knocksideways' method to rapidly and inducibly reroute spindle proteins to nearby mitochondria (Robinson et al., 2010). This allowed us to examine the role of inter-MT bridges at specific stages of mitosis, and particularly, in mature K-fibers following normal assembly of the mitotic spindle. Briefly, the knocksideways (KS) method exploits the binding of mammalian target of rapamycin (mTOR) to a complex of rapamycin bound to FKBP12. Rapamycin binds via the FKBP domain of FKBP12 and this binds the FRB (FKBP and rapamycin-binding) domain of mTOR kinase. KS involves the depletion of the target protein by RNAi and the re-expression of a version of the target protein that is refractory to RNAi and is tagged with the FKBP domain from FKBP12. In the same cells, MitoTrap, a mitochondrially targeted FRB domain is also expressed. Addition of rapamycin induces the heterodimerization of FKBP and FRB domains. This results in the protein of interest being rerouted from one subcellular location to mitochondria on a timescale of seconds (Robinson et al., 2010). If this new localization is incompatible with function, then the protein is inactivated.

TACC3 is an essential non-motor protein that binds the MT polymerase ch-TOG and localizes it to spindle fibers (Gergely et al., 2003; Gergely et al., 2000a; Gergely et al., 2000b; Lee et al., 2001; Piekorz et al., 2002). It was originally proposed that TACC3–ch-TOG are important for promoting spindle assembly by stabilizing MT minus ends at the centrosome or by antagonizing the depolymerizing activity of MCAK (Barr and Gergely, 2008; Kinoshita et al., 2005; Peset and Vernos, 2008). Later, it was found that TACC3–ch-TOG are bound to clathrin (Booth et al., 2011; Fu et al., 2010; Hubner et al., 2010; Lin et al., 2010), and possibly GTSE1 (Borner et al., 2012; Hubner et al., 2010) on kinetochore fibers (K-fibers) of the spindle. Here, TACC3–ch-TOG–clathrin complexes are thought to crosslink MTs by forming inter-MT bridges, suggesting a possible role for this non-motor complex in maintenance of spindle structure (Booth et al., 2011; Cheeseman et al., 2011; Royle, 2012; Royle et al., 2005). A rapid method of inactivation is therefore required to distinguish the role of the TACC3–ch-TOG–clathrin complex in assembly and maintenance of spindle structure. Furthermore, clathrin has distinct functions in

membrane trafficking and centrosome maturation in interphase (Brodsky, 2012) and TACC3 has a role in mRNA translation (Peset and Vernos, 2008). Slow inactivation methods alter these processes, which may cause indirect effects on mitosis and further confuse the interpretation of mitotic phenotypes.

In this study we use KS to remove TACC3–ch-TOG–clathrin complexes from mitotic spindles following normal spindle assembly and chromosome alignment. We find that TACC3–ch-TOG–clathrin complexes are required for the maintenance of K-fiber tension. Our findings demonstrate the utility of KS versus RNAi alone and describe the importance of non-motor proteins in the maintenance of spindle structure and micromechanics beyond initial assembly.

Results

Knocksideways is effective in mitosis for rapid, inducible removal of TACC3 from the mitotic spindle

We began by determining if rapid removal of spindle proteins is feasible during mitosis using knocksideways (KS), and on what timescale it could occur. To do this, we co-transfected HeLa cells with a plasmid to express mCherry-MitoTrap and a pBrain vector that simultaneously depleted endogenous TACC3 via shRNA and re-expressed a shRNA-refractory version of TACC3 that was tagged with GFP and FKBP (Fig. 1A). Live cells at metaphase were identified and imaged, with addition of rapamycin (200 nM) after 3 minutes (supplementary material Movie 1; Fig. 1B). We observed the removal of GFP-FKBP-TACC3 from the metaphase spindle within ~5 minutes of rapamycin application, and its colocalization to the mitochondria surrounding the spindle (Fig. 1B,C). Rerouting of GFP-FKBP-TACC3 to mitochondria was slower than in interphase, where rerouting followed a double exponential decay (Fig. 1D). We suspect that this difference is due to absence of a spindle in interphase to which TACC3 binds. By comparison, GFP-FKBP was rerouted extremely rapidly to mitochondria in interphase and at metaphase (Fig. 1D).

In a typical KS experiment we used four conditions, three controls and one test condition (Fig. 2A). In vehicle-treated cells, GFP-FKBP-TACC3 remained unaltered; and in cells expressing GFP-TACC3 without the FKBP domain, localization was unaffected by vehicle or rapamycin addition (Fig. 2A; supplementary material Fig. S1).

We found that effective rerouting of TACC3 KS depended on co-transfection of both plasmids and good expression of MitoTrap, which must be present in excess. For the method to be useful, the levels of TACC3 prior to KS must be within the normal range and after KS, the levels must be comparable to RNAi or Aurora A inhibition with MLN8237 (Booth et al., 2011). We assessed the levels of TACC3 on the spindle and in the cytoplasm for all conditions (Fig. 2B). This analysis showed that our re-expression of shRNA-refractory TACC3 in cells depleted of endogenous TACC3 was equivalent to endogenous levels and was not overexpressed (Fig. 2B). In addition, TACC3 KS resulted in a lower level of TACC3 at the spindle compared to RNAi or Aurora A inhibition.

TACC3 KS specifically removes the entire TACC3–ch-TOG–clathrin complex from the mitotic spindle

We next asked whether the rapid removal of TACC3 from the spindle affected other spindle proteins. To answer this question, we tested for rerouting of a number of other spindle proteins

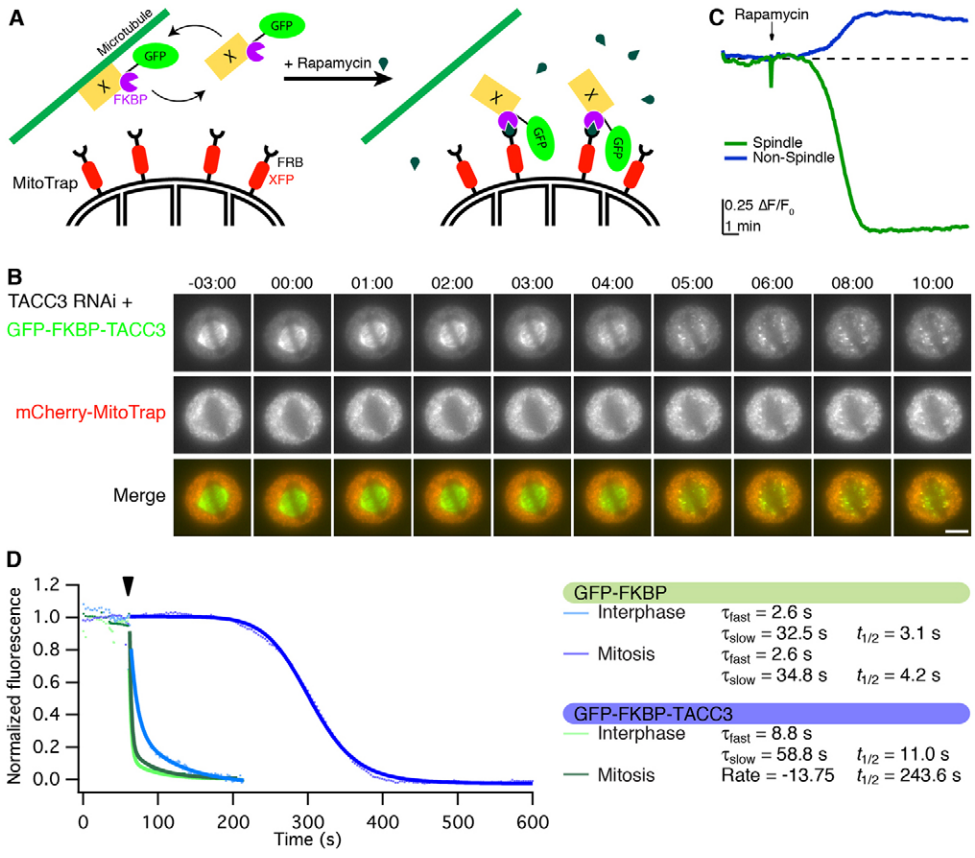

Fig. 1. Rapid, induced removal of TACC3 by knocksideways. (**A**) Diagram of knocksideways of a microtubule-associated protein. Protein X is depleted by RNAi and a shRNA-refractory version is re-expressed. Left: In the absence of rapamycin, the recombinant GFP- and FKBP-tagged protein X cycles on and off the microtubule. Right: Upon addition of rapamycin, the FKBP domain heterodimerizes with the FRB of XFP-MitoTrap (red) located on the mitochondria. (**B**) Video stills of TACC3 KS in a metaphase HeLa cell. Rapamycin (200 nM) was added at time zero (time is shown in minutes:seconds). GFP-FKBP-TACC3 is completely removed in ~5 minutes. Scale bar: 10 µm. (**C**) Quantification of GFP $\Delta F/F_0$ in the indicated areas over time during TACC3 KS. See supplementary material Movie 1. (**D**) Comparison of rerouting kinetics for GFP-FKBP-TACC3 or GFP-FKBP to mitochondria in interphase or mitosis, single cell examples. An overlay of curve fits to describe the rerouting are shown on the same time scale. Rapamycin application is denoted by the arrowhead. GFP-FKBP-TACC3 in mitosis was best fit by the Hill logistic function, all other data were best fit by a double exponential function.

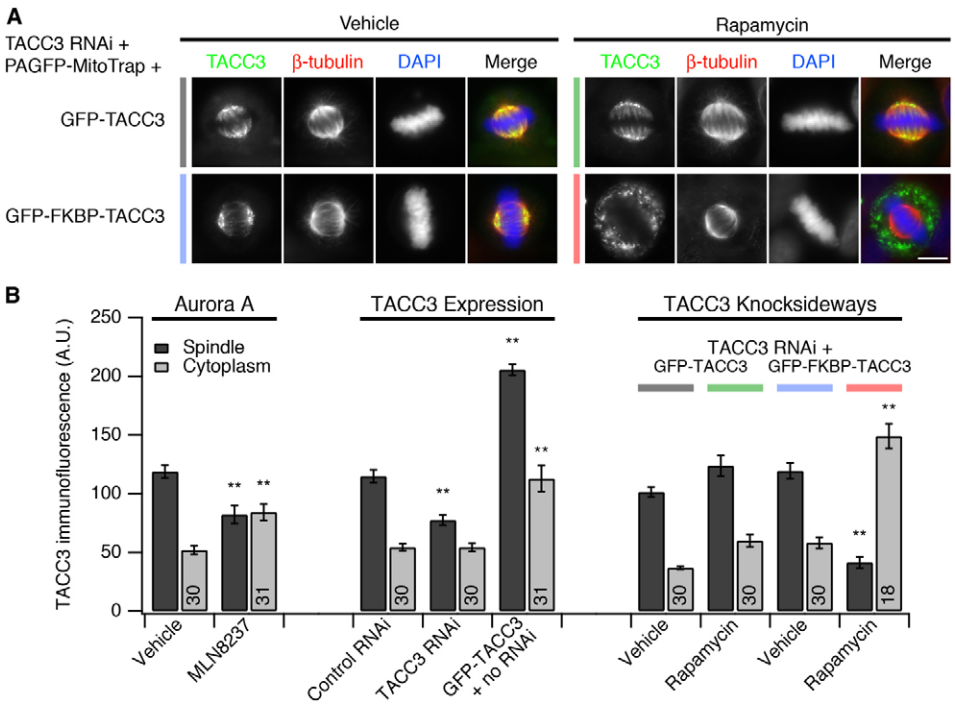

Fig. 2. Removal of TACC3 from mitotic spindles by knocksideways. (**A**) Representative micrographs of TACC3 KS. TACC3-depleted cells expressing PAGFP-MitoTrap (not visible) and the indicated TACC3 construct were treated for 30 minutes with 200 nM rapamycin or vehicle, fixed and stained for tubulin. Color coding for KS conditions is used throughout the paper. Full results are shown in supplementary material Fig. S1. Scale bar: 10 µm. (**B**) Bar chart to show quantification of TACC3 immunofluorescence in various experimental conditions. Total TACC3 was detected using anti-TACC3/A568 and analyzed by confocal microscopy. Aurora-A inhibition: using MLN8237 (1 µM) compared to vehicle. TACC3 expression: control RNAi + GFP, TACC3 RNAi + GFP and GFP-TACC3 expression (with no RNAi). TACC3 KS: TACC3 RNAi + PAGFP-MitoTrap + GFP-TACC3 or GFP-FKBP-TACC3; treated with vehicle or rapamycin (200 nM). Mean ± s.e.m. for spindle regions and cytoplasm. Number of cells was 18–31 as indicated, from two experiments. $^{**}P<0.001$ compared with vehicle (far left) values, one-way ANOVA with Tukey–Kramer post-hoc test.

following 10 minutes of rapamycin application (Fig. 3). Indirect immunofluorescence showed that TACC3 KS caused the removal of clathrin and ch-TOG from the spindle. In both cases, clathrin and ch-TOG were found colocalized with TACC3 at the mitochondria. Interestingly, GTSE1, a protein reported to be part of the TACC3–ch-TOG–clathrin complex (Hubner et al., 2010; Royle, 2012), was also lost from the spindle following TACC3 KS, although it was difficult to detect co-rerouting of GTSE1 at mitochondria (Fig. 3). Normal localizations of ch-TOG, clathrin and GTSE1 were observed in control cells, where GFP-FKBP-TACC3 was expressed and vehicle-treated (Fig. 3) or where GFP-TACC3 (without an FKBP domain) was expressed and cells treated with either rapamycin or vehicle (supplementary material Fig. S1). We also examined NuMA, Eg5 and HURP, as

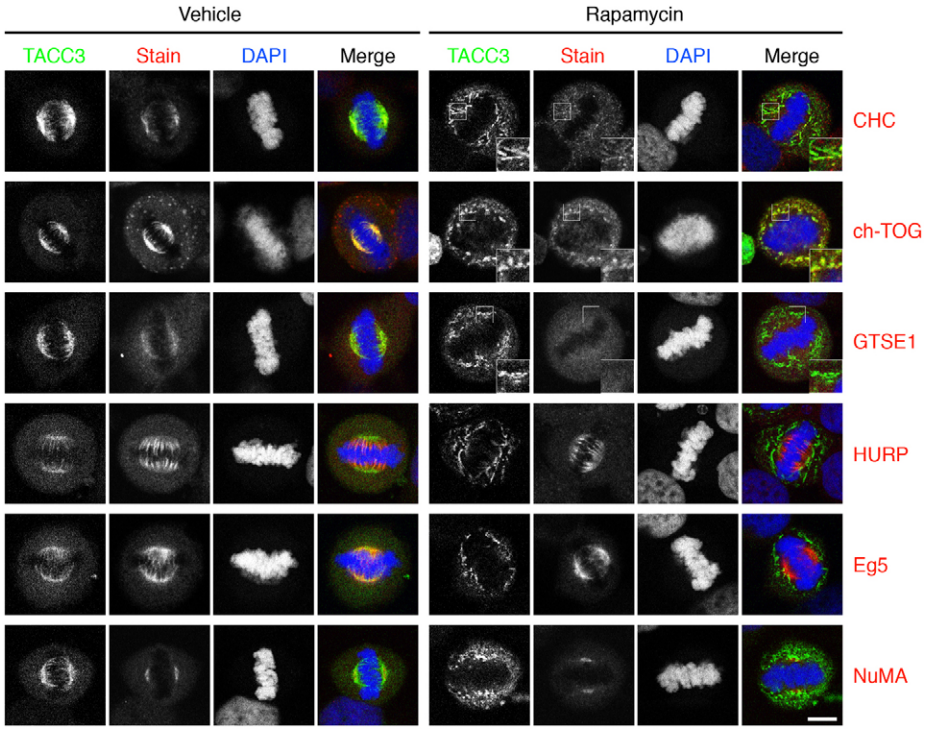

Fig. 3. TACC3 KS removes ch-TOG, clathrin and GTSE1 from the spindle without affecting other spindle proteins. Representative confocal micrographs of TACC3-depleted HeLa cells in metaphase expressing GFP-FKBP-TACC3 (green) and PAGFP-MitoTrap (not visible) that were treated with vehicle or rapamycin (200 nM) for 10 minutes, fixed and stained for the indicated proteins (red). TACC3 KS removed ch-TOG, clathrin heavy chain (CHC) and GTSE1 from the spindle. NuMA, HURP and Eg5 were unaffected by TACC3 KS. Zoomed areas show the colocalization of proteins at mitochondria following TACC3 KS. The results are typical of this experiment, repeated four times. See supplementary material Fig. S1 for full results. Scale bar: 10 µm.

these proteins localize to different areas of the spindle yet require phosphorylation by Aurora-A kinase for their activity, similarly to TACC3 (Giet et al., 1999; Kettenbach et al., 2011; Yu et al., 2005). The localization of all three proteins was unaltered by TACC3 KS (Fig. 3). We also tested whether TACC3 removal from the spindle would eventually cause deficiencies after prolonged drug application. The results of these experiments, with 30 minutes of drug application, were very similar to those with 10 minutes application (supplementary material Fig. S1). TACC3 KS is therefore a useful method to remove TACC3–ch-TOG–clathrin complexes specifically from spindles on a rapid timescale and that this will allow the molecular dissection of TACC3–ch-TOG–clathrin function at different stages of mitosis.

Rerouting clathrin to mitochondria is equivalent to TACC3 KS

We also used a similar system to reroute clathrin from the spindle to mitochondria during mitosis (supplementary material Fig. S2). Removal occurred with similar kinetics to TACC3 KS (supplementary material Movie 2). Analysis of spindle protein localization showed that rerouting of clathrin also removed members of the TACC3–ch-TOG–clathrin complex including GTSE1, whereas Eg5, NuMA and HURP were unaffected (supplementary material Fig. S2). In cells with good rerouting of clathrin to mitochondria, TACC3 was completely colocalized with clathrin on the mitochondria (supplementary material Fig. S3). TACC3 was lost from spindle microtubules and centrosomes, even in early mitosis, arguing against the existence of a clathrin-independent pool of TACC3. However, due to the abundance of clathrin in the cell, we could not rule out the possibility that clathrin removal in some cells may be incomplete (supplementary material Fig. S2). Therefore TACC3 KS was used to remove TACC3–ch-TOG–clathrin in all subsequent experiments.

TACC3 KS causes loss of a subpopulation of inter-MT bridges in K-fibers

K-fibers are bundles of parallel MTs that are crosslinked by inter-MT bridges (Hepler et al., 1970; McDonald et al., 1992; Nicklas et al., 1982). Previously, we showed that TACC3–ch-TOG–clathrin complexes form a subset of inter-MT bridges in K-fibers (Booth et al., 2011; Cheeseman et al., 2011; Royle, 2012; Royle et al., 2005). We next used correlative light-electron microscopy (CLEM) to verify if removal of TACC3–ch-TOG–clathrin complexes by KS resulted in a concomitant loss of inter-MT bridges. To do this, metaphase cells expressing GFP-FKBP-TACC3 and mCherry-MitoTrap were identified by fluorescence microscopy, and rapamycin (200 nM) or vehicle was applied for 10 minutes. TACC3 KS was visualized and the cells were then fixed and processed (Fig. 4A). The target cell was relocated in the resin and sectioned longitudinally relative to the spindle axis, and imaged by EM (Fig. 4A). Inter-MT bridges were quantified as previously described (Booth et al., 2011) (Fig. 4B). We found that there was a significant loss of inter-MT bridges in K-fibers after 10 minutes of TACC3 KS (Fig. 4C). This indicates that the removal of TACC3–ch-TOG–clathrin complexes from spindles by TACC3 KS results in removal of some inter-MT bridges. Many bridges clearly remain and these bridges must be composed of other proteins. With a method to inducibly and specifically remove TACC3–ch-TOG–clathrin bridges in hand we could investigate the role of these structures in K-fibers at different stages of mitosis.

Removal of TACC3–ch-TOG–clathrin complexes at NEBD or after metaphase reveals two different aspects of crosslinking function

Our next aim was to use live-cell imaging and TACC3 KS to assess the role of TACC3–ch-TOG–clathrin inter-MT bridges at different stages in mitosis. For reference, TACC3 KS was compared with depletion of TACC3 by RNAi. Progression through mitosis of live HeLa cells expressing mCherry-H2B was visualized and the time from NEBD-to-metaphase and from metaphase-to-anaphase was measured (Fig. 5A). In agreement with previous studies, depletion of TACC3 by RNAi prolonged the time from NEBD to metaphase and the time from metaphase to anaphase, relative to untransfected cells (Gergely et al., 2003; Lin et al., 2010; Schneider et al., 2007) (Fig. 5B). These defects

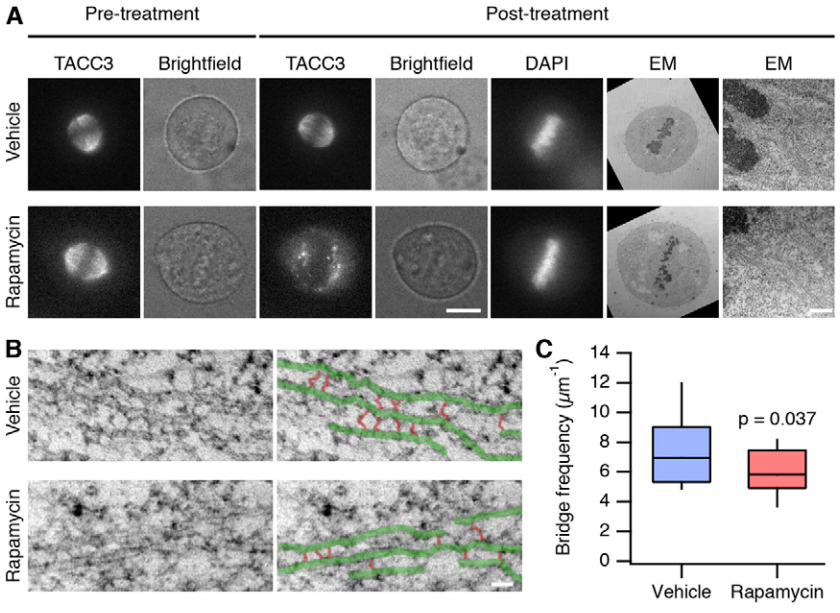

Fig. 4. Loss of inter-microtubule bridges from K-fibers following TACC3 KS. (**A**) TACC3-depleted HeLa cells at metaphase expressing GFP-FKBP-TACC3 and mCherry-MitoTrap were treated with rapamycin (200 nM) or vehicle for 10 minutes, fixed and processed for CLEM. The cell was located, 80-nm longitudinal sections taken (EM) and the bridge frequency in K-fibers quantified. Scale bars: 10 µm (left) and 500 nm (right). (**B**) Example micrographs to show visualization of inter-MT bridges for quantification. Annotated micrograph (right) shows MTs (green) and bridges (red). Scale bar: 50 nm. (**C**) Tukey box plot of inter-MT bridge frequency in K-fibers, expressed per micron of total MT length. In TACC3 KS cells, a significant loss of MT crosslinkers was observed: control $n=4$ cells (20 sections), TACC3 KS $n=5$ cells (25 sections); Student's t-test, $P=0.037$.

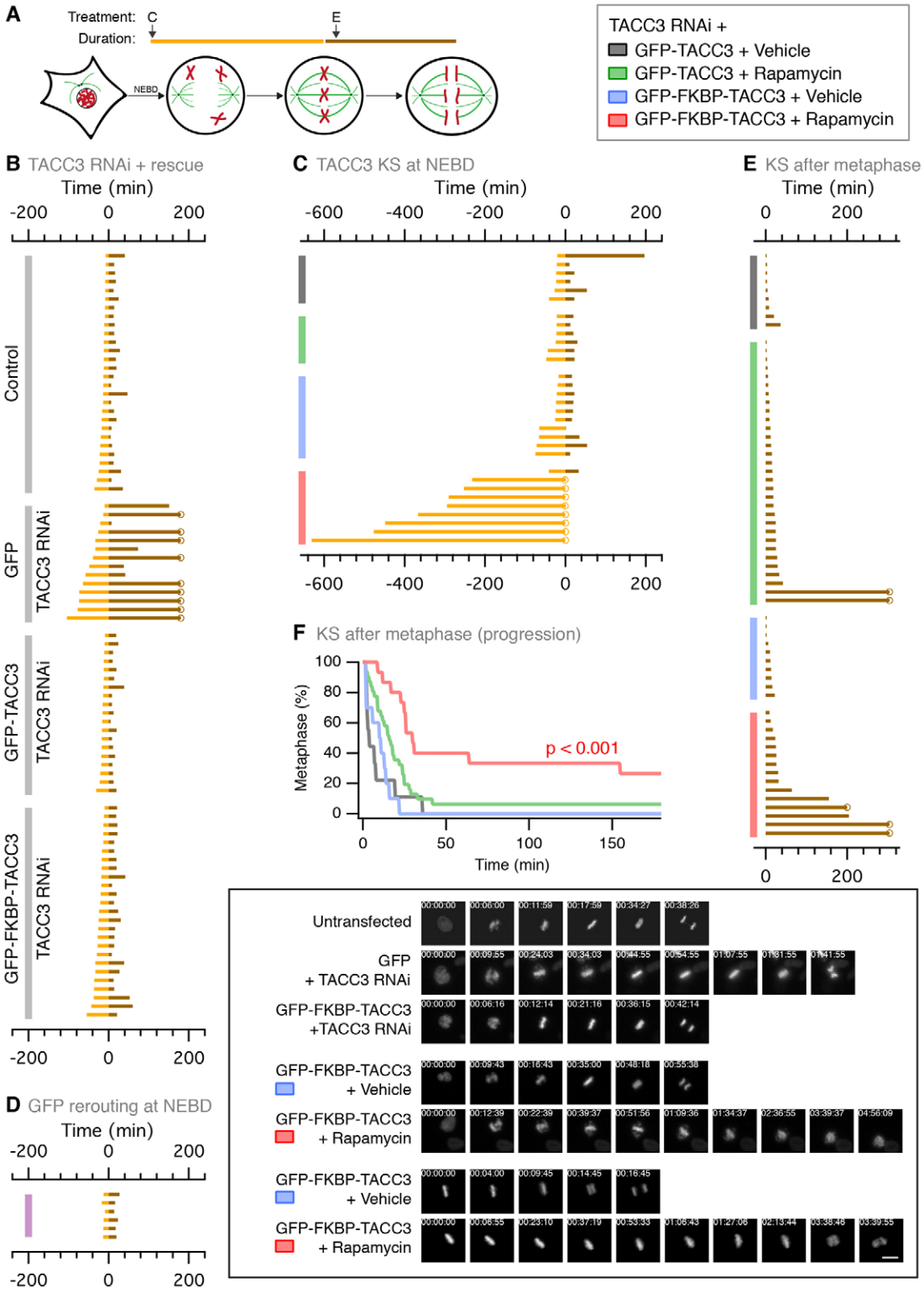

Fig. 5. TACC3 KS at NEBD or after metaphase reveals two different aspects of crosslinking function. (**A**) Diagram to show the timing of mitosis and experimental conditions. (**B**) Mitotic progression of control cells (no RNAi) and TACC3-depleted cells expressing GFP, GFP-TACC3 or GFP-FKBP-TACC3. TACC3 RNAi caused delay in chromosomal alignment in HeLa cells (NEBD-to-metaphase timing, gold) and also a delay in anaphase onset (metaphase-to-anaphase timing, brown). Cells that did not reach anaphase within the movie are marked with a circle. (**C**) Mitotic progression of TACC3-depleted HeLa cells expressing GFP-TACC3 or GFP-FKBP-TACC3; either vehicle or rapamycin (200 nM) was added at NEBD. (**D**) Normal mitotic progression of cells where GFP-FKBP was rerouted to mitochondria at NEBD. (**E**) Similar graph as in C except that TACC3 KS was performed after metaphase. All cells in the figure coexpressed H2B-mCherry for chromosome visualization and PAGFP-MitoTrap. (**F**) 'Survival curves' of the data shown in E. Example video stills from the indicated conditions are shown in the boxed area. Timings are indicated in hh:mm:ss. Scale bar: 20 µm.

were rescued by re-expression of shRNA-refractory GFP-TACC3 or GFP-FKBP-TACC3 (Fig. 5B), which indicates that the RNAi phenotype is specific to depletion of TACC3 and that our constructs are functional when expressed in cells depleted of TACC3. Delayed progression to anaphase in TACC3-depleted cells could be due to a role for MT crosslinking in K-fiber function at metaphase or simply a defect that is secondary to the prolonged prometaphase. These possibilities could now be distinguished using KS.

We next tested the effect of TACC3 KS at NEBD. To do this, live HeLa cells expressing PAGFP-MitoTrap, mCherry-H2B and TACC3 shRNA together with either GFP-TACC3 or GFP-FKBP-TACC3, were imaged with either vehicle or rapamycin added at NEBD. TACC3 KS at NEBD resulted in a severely prolonged prometaphase (Fig. 5C). The defects in chromosome alignment were so extreme that most TACC3 KS cells did not attain metaphase within several hours of imaging (Fig. 5C). The three control groups had normal prometaphase and subsequent metaphase-to-anaphase timings indicating that the effect of TACC3 KS was indeed due to removal of TACC3-containing complexes and not to application of rapamycin itself. This suggests that TACC3–ch-TOG–clathrin complexes are essential for an efficient and successful prometaphase, a time when the K-fiber matures.

TACC3 KS at NEBD produced a much stronger phenotype than TACC3 RNAi. To rule out the possibility that loading protein onto mitochondria delays mitosis non-specifically (‘neomorphic’ phenotype), we tested the effect of rerouting GFP-FKBP to mitochondria at NEBD. In six out of six cells, no delay was seen in NEBD–metaphase or in metaphase–anaphase timing (Fig. 5D). Furthermore, in TACC3 KS experiments, mitotic entry did not appear blocked in neighboring G2 cells. These observations indicate that the stronger phenotype upon rapid removal of TACC3 (compared to TACC3 RNAi), reflects a genuine difference between the methodologies.

To test the effect of TACC3–ch-TOG–clathrin complexes in mature spindles, we performed the same experiments but applied rapamycin after all chromosomes had aligned. These cells had therefore undergone a normal prometaphase and attained metaphase. Any changes caused by TACC3 KS would only be the result of TACC3–ch-TOG–clathrin loss from mature spindles and not from problems earlier in mitosis. TACC3 KS after metaphase caused a delay in anaphase onset (Fig. 5E), when compared with the three control groups (Fig. 5F). This indicates that removal of this complex from mature spindles at metaphase results in perturbed K-fiber function. Thus, TACC3–ch-TOG–clathrin inter-MT bridges are important for the function of mature K-fibers as well as having essential roles earlier in mitosis, e.g. in spindle assembly.

TACC3 KS during metaphase reduces K-fiber tension and this is sensed by the spindle checkpoint

We next investigated the cause of the metaphase-to-anaphase delay that resulted from TACC3 KS at metaphase. First, we assessed the spindle checkpoint by quantifying Mad2-positive kinetochores in metaphase cells following rapamycin treatment (30 minutes). The number of Mad2 immunoreactive puncta per cell that colocalized with the anti-centromere antibody CREST was quantified (Fig. 6A,B). The proportion of cells containing no Mad2-positive kinetochores was decreased by 40% following

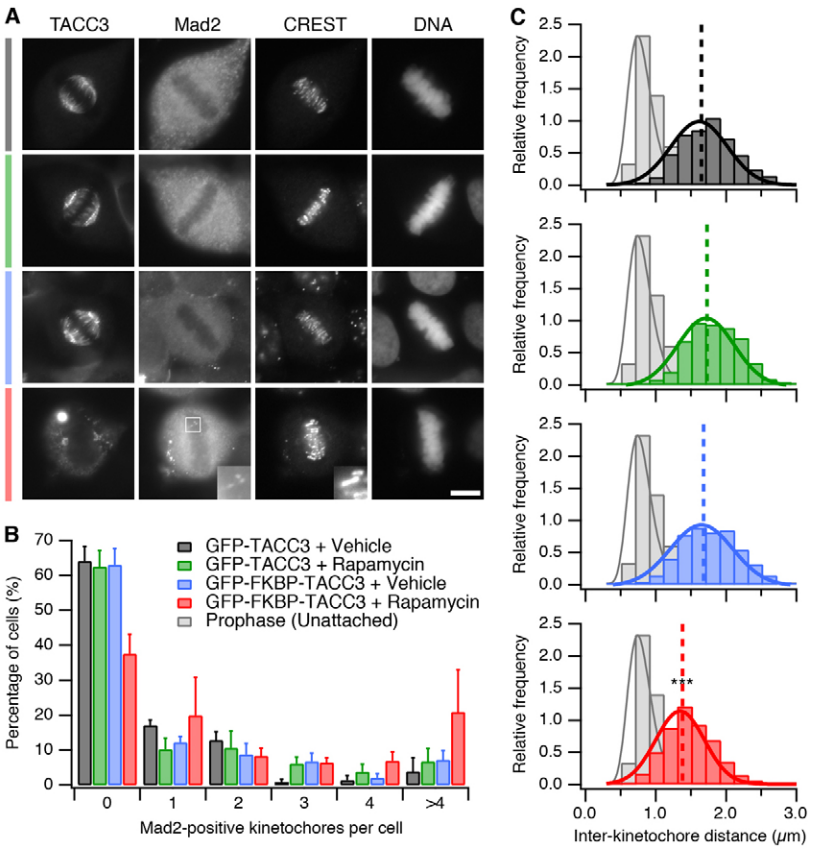

Fig. 6. TACC3 KS at metaphase reduces K-fiber tension and cells are arrested by the spindle checkpoint. (**A**) Representative confocal micrographs to show the recruitment of Mad2 to kinetochores following TACC3 KS. TACC3-depleted HeLa cells expressing GFP-TACC3 or GFP-FKBP-TACC3 were treated as indicated in the key in B. Inset shows three Mad2-positive kinetochores (2.5× zoom). Scale bar: 10 μm. (**B**) Proportion of cells with a satisfied or active spindle checkpoint, as revealed by Mad2 presence at kinetochores. Bars show mean ± s.e.m. of three experiments (n=90–93 cells). (**C**) Histograms of inter-kinetochore distances. Histograms (colored according to the key in B) are shown for GFP-TACC3 or GFP-FKBP-TACC3 treated with vehicle or rapamycin (200 nM) for 30 minutes, overlaid on a histogram of unattached inter-kinetochore distances from prophase/early prometaphase cells (light grey). The mean inter-kinetochore distance is shown by a dashed line. The unattached data were fitted with a log-normal function and all other data were fitted with a single Gaussian function. TACC3 KS cells (red, n=645 from 20 cells) displayed significantly reduced inter-kinetochore distance compared with controls (grey, n=654 from 22 cells; green, n=656 from 23 cells; blue, n=578 from 23 cells), but was not significantly different from unattached kinetochores (n=238 from 8 cells); ***P<0.001.

TACC3 KS compared to controls (Fig. 6B). In addition, the proportion displaying >4 Mad2-positive kinetochores was increased 3-fold following the removal of TACC3–ch-TOG–clathrin inter-MT bridges from K-fibers (Fig. 6B). Second, we assessed the effect of TACC3 KS on K-fiber tension by measuring inter-kinetochore distances. After rapamycin application (30 minutes), we observed a decrease in the mean ± s.d. inter-kinetochore distance from 1.68±0.06 μm (vehicle) to 1.38±0.04 μm (rapamycin). This suggested that the kinetochores were still attached but were under less tension because in prometaphase cells, unattached kinetochores had a mean inter-kinetochore distance of 0.83±0.06 μm (Fig. 6C). The distribution of inter-kinetochore distances showed an overall shift to lower values following TACC3 KS with no emergence of a second population around 0.6–1 μm suggesting no loss of attachment following TACC3 KS (Fig. 6C). Together, these results indicate that the slowed progression to anaphase following TACC3 KS was due to spindle checkpoint signaling. As the control cells had silenced the checkpoint satisfactorily and maintained tension, we interpret this to mean that the spindle checkpoint had been 're-activated' and that this re-activation was due to a loss of K-fiber tension.

TACC3 KS from mature K-fibers causes minimal MT loss

In order to determine whether kinetochores had lost attachment to the spindle following TACC3 KS, we tested the number of kinetochores with cold-stable microtubule attachments in metaphase cells (Fig. 7A,B). In control or TACC3 KS cells, all kinetochores had cold-stable attachment to the spindle. Depletion of Nuf2 served as a positive control to show that we could detect kinetochores that lacked cold-stable attachments (Fig. 7B). TACC3 KS did not significantly alter the remaining tubulin signal in cold-treated cells relative to control cells, which suggested that MT occupancy is normal.

To investigate this further we used CLEM to analyze MT number in K-fibers sectioned orthogonally relative to the spindle axis (Fig. 7C). We found only a small decrease in MT number compared to controls after 10 minutes TACC3 KS, and this remained stable at 30 minutes (Fig. 7D), i.e. there was no progressive loss of MTs ($P>0.05$). Neither of these decreases was statistically significant compared to rapamycin-treated control K-fibers ($P>0.05$), although there was significant decrease when compared to vehicle-treated K-fibers ($P<0.001$). The cross-sectional area of K-fibers was estimated and the relation between K-fiber area and MT number plotted (Fig. 7E). These plots illustrate that after TACC3 KS, MT number per K-fiber is within the normal range, albeit at the lower end. The MT density within K-fibers was equivalent suggesting that any MT loss that occurred following TACC3 KS was limited to the periphery of the fiber. Nearest neighbor analysis and neighbor density analysis both failed to show any effect of TACC3 KS on MT spacing or distribution within K-fibers compared to control cells following 10 or 30 minutes rapamycin application (supplementary material Fig. S3). These results are in contrast to our previous analysis of K-fibers in clathrin RNAi cells, where MT loss occurred throughout the K-fiber (Booth et al., 2011). The difference is likely due to the fact that TACC3 KS was performed at metaphase after the K-fiber had accumulated the correct number of MTs and stabilized them; whereas clathrin-depleted cells may have been unable to accumulate MTs during prometaphase. Together, these results show that the number of attachments and the MT occupancy at kinetochores is normal following TACC3 KS. The mitotic delay and re-activated spindle checkpoint signaling following TACC3 KS indicates that the spindle checkpoint can sense reduced K-fiber tension that occurs without detectable loss of MT attachment.

TACC3 KS from mature K-fibers causes changes in spindle shape and dynamicity

How does removal of TACC3–ch-TOG–clathrin inter-MT bridges result in reduced K-fiber tension? To address this question we examined mitotic spindle dynamics following removal of TACC3–ch-TOG–clathrin complexes, using 4D kinetochore and spindle pole tracking in live HeLa cells stably expressing GFP-CENP-A and centrin-GFP (Fig. 8). TACC3 KS was performed using mCherry-tagged TACC3 constructs at late prometaphase/metaphase. Cells were imaged and time-lapse datasets were analyzed as previously described (Jaqaman et al., 2010) and also with a new algorithm (see Materials and Methods), allowing kinetochore and spindle pole motions to be tracked in an automated manner (Fig. 8).

Removal of TACC3–ch-TOG–clathrin complexes by TACC3 KS resulted in a number of changes in kinetochore dynamics. First, kinetochore oscillations in typical trajectories from TACC3 KS cells were visibly dampened compared to controls (Fig. 8A–C). Second, inter-kinetochore distance was reduced by ~10% (Fig. 8D,E) confirming in live cells our earlier observations in fixed cells that K-fiber tension was decreased despite normal MT occupancy. Third, the metaphase plate was thicker following TACC3 KS, as the distance of sister kinetochore centers was more variable than in cells without TACC3 removal (Fig. 8E; Bartlett's statistic, 87.799, $P<0.001$). Note, that this variability is likely much larger as the analysis rejects kinetochores where $x>2.5\sigma$. Fourth, auto-correlation analysis of sister center displacement (Δx) showed that kinetochore oscillations had a reduced periodicity following TACC3 KS (Fig. 8F), whereas sister displacement cross-correlation analysis showed no alteration of kinetochore 'breathing' by TACC3 KS. Fifth, mean squared displacement analysis for kinetochore pairs showed that movement of kinetochores following TACC3 KS was less constrained compared to controls (Fig. 8G). In other words, for a given duration, kinetochores have moved further following TACC3 KS than in cells with normal levels of TACC3 on the spindle. This observation is in agreement with the increased variability in x (Fig. 8E). All of these changes in kinetochore dynamics following TACC3 KS during metaphase are consistent with a decrease in K-fiber tension.

We also analyzed the motions of spindle poles in the same cells using automated tracking (Fig. 8H). This analysis revealed that the pole-to-pole distance of spindles was reduced by ~12% following TACC3 KS (Fig. 8I). This decrease in spindle length (S), which was noted previously (Fig. 2A), was the only detectable change in spindle pole dynamics. The movement of spindle poles is random, i.e. they do not undergo oscillations over time; and there was no alteration in the mean squared displacement (m.s.d.) of spindle poles following TACC3 KS. The average inter-kinetochore distance (d) was plotted as a function of the average pole-to-pole distance (S) for each cell analyzed across four experiments (Fig. 8J). This showed that the d and S did not scale with one another and argues that the decrease in d is not caused by the reduction in S. These results indicate that removal of TACC3–ch-TOG–clathrin complexes

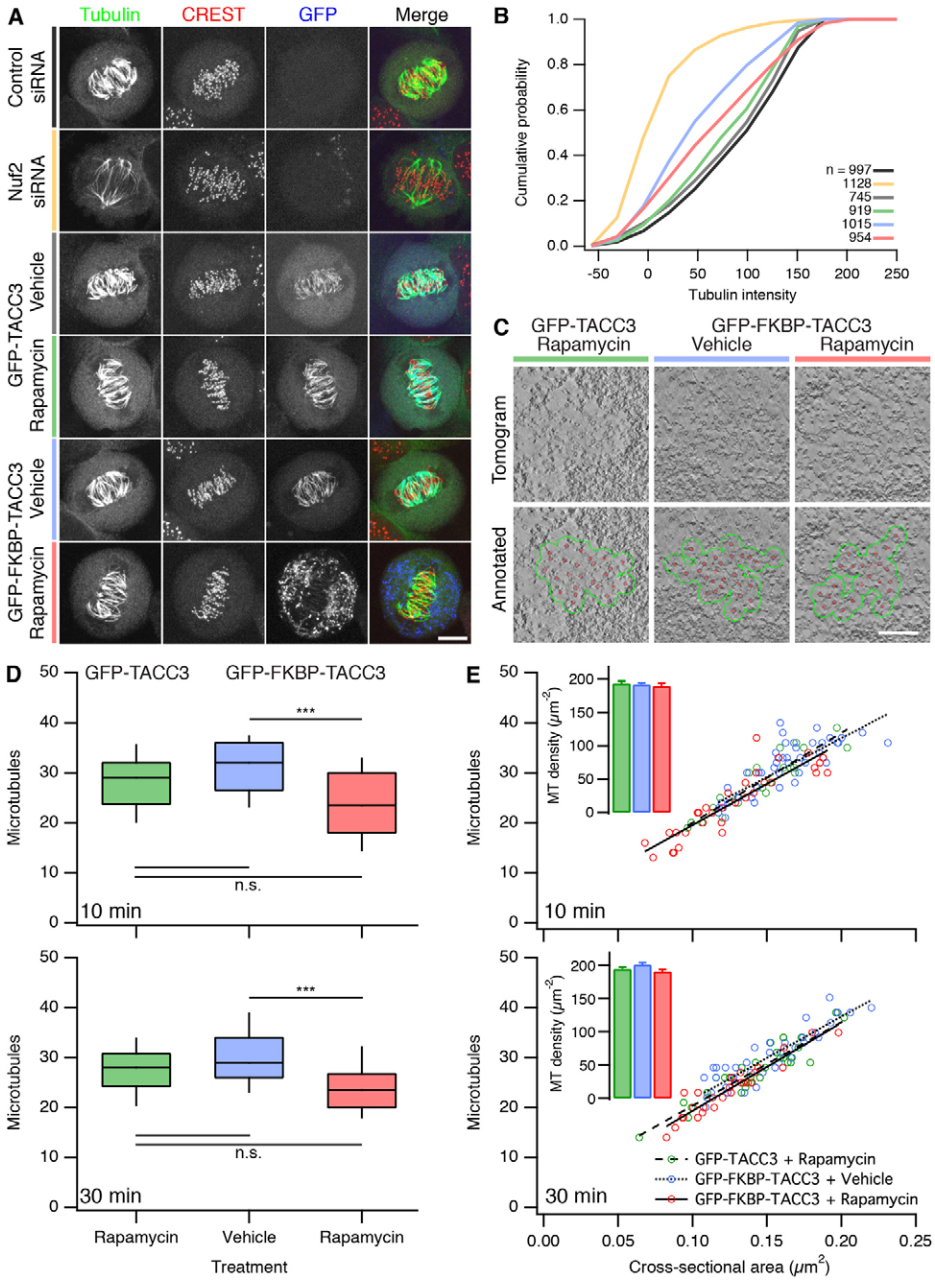

Fig. 7. TACC3 KS at metaphase does not significantly alter kinetochore–microtubule attachments. (**A**,**B**) Cold-stable kinetochore–microtubule attachments. (A) Representative pictures of each condition analyzed are shown as maximum intensity projections of confocal Z-series micrographs. Metaphase cells were cold-treated, fixed and stained with anti-tubulin (green) and CREST (red); GFP channel (blue) shows TACC3 KS. Scale bar: 10 µm. (B) Analysis of confocal z-series micrographs to detect cold-stable kinetochore–microtubule attachments. Cumulative frequency plot to show the average tubulin signal adjacent to kinetochores. N_{cell}=9–12 from two experiments. $N_{kinetochore}$ is shown in the legend. (**C**) Representative views of electron tomograms of orthogonal sections of K-fibers in metaphase HeLa cells expressing mCherry-MitoTrap and GFP-TACC3 or GFP-FKBP-TACC3 treated as indicated. Overlaid are microtubules (red) and the calculated K-fiber perimeter (green). Scale bar: 100 nm. (**D**) Tukey box plots of K-fiber MT number in TACC3-depleted HeLa cells expressing mCherry-MitoTrap and GFP-TACC3 or GFP-FKBP-TACC3, treated with vehicle or rapamycin (200 nM) for 10 minutes (top) or 30 minutes (bottom). TACC3 KS (red) causes a slight reduction in MTs of K-fibers after both 10 minutes and 30 minutes of rapamycin application. The reduction was significantly lower than for vehicle-treated cells (ANOVA with Tukey–Kramer post-hoc test, ***P<0.01), but not when compared with rapamycin-treated GFP-TACC3-expressing cells (n.s. indicates P>0.05). (**E**) Plots of MT number versus K-fiber cross-sectional area after 10 minutes and 30 minutes of treatment. Lines of best fit show the similar MT density in all conditions. Insets show mean ± s.e.m. K-fiber MT density in control (green, blue) or TACC3 KS cells (red) (10-minute data: green, n=22 K-fibers; blue, n=54; red, n=32. 30-minutes data: green, n=32; blue, n=38; red, n=28). See supplementary material Fig. S4 for spatial analysis of K-fibers.

from mitotic spindles that had completed a normal prometaphase caused the following changes: reduced spindle length, reduced K-fiber tension and decreased micromechanics of the spindle.

Discussion

We investigated the requirement for one class of non-motor MT crosslinker (TACC3–ch-TOG–clathrin) for the function of mature K-fibers. Such an investigation was made possible by the knocksideways technique which allowed the inducible, rapid removal of certain inter-MT bridges from K-fibers at different stages of mitosis. Our findings demonstrated the utility of KS versus RNAi and a role for TACC3–ch-TOG–clathrin complexes in the shape and micromechanics of mature spindles.

The advantages of KS over RNAi are clear, given that protein depletion via RNAi is slow (24–72 hours) compared to the timescale of mitosis (1–2 hours). Using RNAi, attempts to determine the function of a spindle protein are complicated because the cell may have undergone several cell cycles with gradually declining levels of the protein. In this time, the cell may upregulate alternative pathways to compensate for the reduced protein, potentially masking the true phenotype. For spindle proteins with distinct interphase functions the picture is further complicated (Royle, 2011). In addition, trying to understand RNAi phenotypes at later stages of mitosis are potentially confounded by earlier defects. In other words, is the phenotype caused by a true requirement for the depleted protein at that later stage or is it because the earlier absence of the protein produced a defective spindle? It is now possible to dissect these differences using KS. Rapid inactivation methods are particularly crucial for mitosis, which is a succession of steps, each lasting less than 30 minutes.

The effectiveness of KS on a timescale of ~5 minutes makes it better suited than methods for inducible protein degradation, which work on the timescale of 30 minutes (Nishimura et al., 2009). Besides the use of KS as a tool for protein inactivation (Hirst et al., 2012; Robinson et al., 2010), we showed indirectly two additional uses for the method. First, the lifetime of proteins on the spindle could be inferred by comparing the kinetics of rerouting in mitotic and interphase cells. Second, testing which proteins are co-rerouted to mitochondria upon KS is a useful way to determine which proteins bind one another in cells.

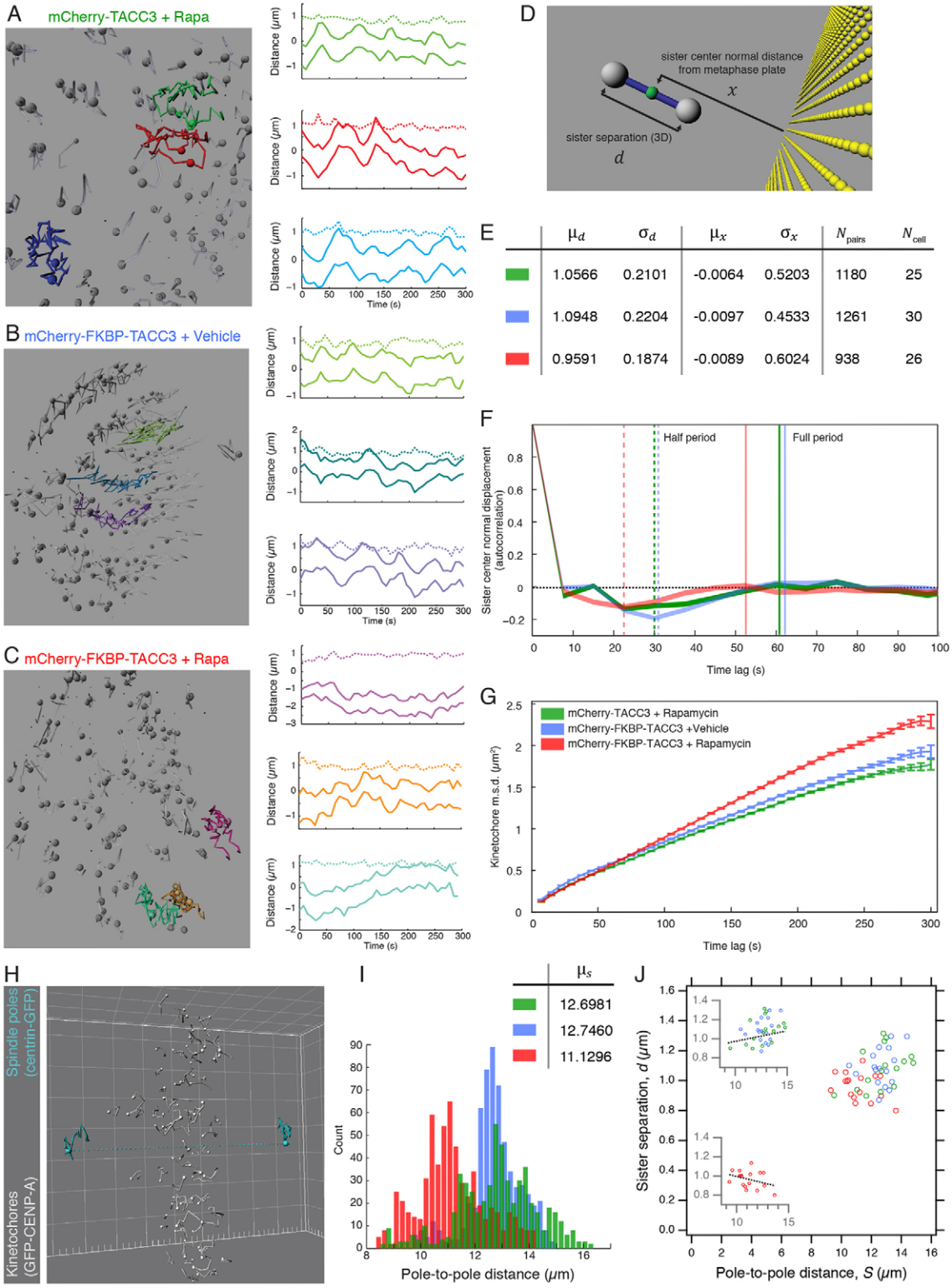

Fig. 8. See next page for legend.

TACC3 KS caused the specific rerouting of ch-TOG and clathrin from the spindle to mitochondria. Importantly, these partners were co-rerouted with TACC3 to the mitochondria, rather than being simply lost from the spindle, unable to bind in the absence of TACC3. This observation indicates that TACC3 KS reroutes the intact TACC3–ch-TOG–clathrin complex. Moreover, the co-rerouting suggests that interactions within the complex, for example between clathrin and TACC3, are of higher affinity than clathrin–adaptor interactions, as it was shown previously that AP-2 KS did not co-reroute clathrin to mitochondria (Robinson et al., 2010). We note that a pool of ch-TOG was retained at the spindle pole after TACC3 KS (supplementary material Fig. S1), which presumably corresponds to a functionally separate ch-TOG population, as previously described (Booth et al., 2011; Cassimeris et al., 2009; Gergely et al., 2003). Since the discovery of clathrin as a binding partner of TACC3–ch-TOG, it has been debated whether TACC3–ch-TOG can operate independently of this complex (Booth et al., 2011; Fu et al., 2011; Fu et al., 2010; Hubner et al., 2010; Lin et al., 2010; Royle, 2012). Co-rerouting of TACC3 and clathrin was complete, indicating that these proteins do not exist as functionally separate entities at the spindle and are probably interdependent for their recruitment to the spindle (Royle, 2012).

TACC3 KS caused the loss of some inter-MT bridges. However, we found that the extent of loss following TACC3 KS was less than that observed after RNAi of TACC3 or clathrin (Booth et al., 2011) or after inhibition of Aurora-A kinase using MLN8237–Alisertib (Cheeseman et al., 2011). As KS is a more rapid and specific method for protein inactivation, we interpret this to mean that our previous analyses overestimated the size of this population of inter-MT bridge. If correct, this points to secondary effects of RNAi or Alisertib beyond the simple removal of TACC3–ch-TOG–clathrin complexes. For example, clathrin-depleted K-fibers had fewer MTs than control RNAi and this could have confounded the quantification of bridge frequency (Booth et al., 2011). As noted previously, many crosslinkers remain in the K-fiber following TACC3 KS and this underscores that other inter-MT bridges exist in K-fibers that are not composed of TACC3–ch-TOG–clathrin.

Using TACC3 KS to remove TACC3–ch-TOG–clathrin inter-MT bridges at metaphase, following a normal prometaphase, we observed delays in the progression to anaphase. We found a net decrease in K-fiber tension despite normal MT attachment and that this state was detected by the spindle checkpoint. These observations could be taken as evidence that the spindle checkpoint can sense K-fiber tension, distinctly from MT attachment (Khodjakov and Pines, 2010). However, the number of Mad2-positive kinetochores was only a small fraction of the total kinetochores despite an overall shift to lower tension at all kinetochores. This result is similar to delayed progression to anaphase in taxol-treated PtK1 cells, where tension is reduced, MT attachment is normal, but Mad2 is only recruited to a subset of kinetochores (McEwen et al., 1997; Waters et al., 1998). The range of MTs/fiber had a tendency to be lower after TACC3 KS and so it is difficult to exclude the possibility that Mad2 is recruited to those kinetochores with fewest MTs.

The decrease in inter-kinetochore distance following TACC3 KS was 10%, while the decrease in pole–pole distance was ~12%. Although these changes are equivalent, several observations suggest that the decreases in inter-kinetochore distance are due to loss of K-fiber tension rather than being simply scaled with spindle size. First, experimental manipulation of pole–pole distance and the resultant change of spindle size have little effect on kinetochore separation (Dumont and Mitchison, 2009). Second, MT crosslinkers increase the tensile strength of MT bundles *in vitro* (Charlebois et al., 2011) and so the removal of a crosslinker is consistent with decreased K-fiber tension. Third, we saw changes in the dynamicity of the spindle and behavior of kinetochores, which argues that TACC3 KS affects the micromechanical properties of the K-fibers in addition to spindle size. Finally, plots of the average inter-kinetochore distance versus pole-to-pole distance showed that these two measures were independent.

One further surprising finding was the magnitude of mitotic delay induced by TACC3 KS at NEBD. This manipulation was predicted to be equivalent to TACC3 RNAi, but was far more severe. Using RNAi, TACC3-depleted cells had a delayed prometaphase but did eventually align their chromosomes. By contrast, cells with TACC3 KS at NEBD were unable to align the chromosomes at all. Four possibilities to explain this difference are: (i) TACC3-depleted cells may have time to compensate for the loss of TACC3 during the depletion period; (ii) removal of TACC3 from spindles by KS may be more extensive than RNAi, due to dimerization of GFP-FKBP-TACC3 with residual TACC3; (iii) rerouting of the whole TACC3–ch-TOG–clathrin complex may result in a significant fraction of ch-TOG and clathrin being trapped on mitochondria and thus unavailable for potential functions that are independent of the complex; (iv) a 'neomorphic' phenotype, where loading mitochondria with heterologous proteins delays mitosis non-specifically. This latter possibility was ruled out by the normal NEBD–anaphase times for cells with rerouting of GFP-FKBP and the observation that TACC3 KS does not impede mitotic entry. Quantification of TACC3 levels on spindle MTs following KS versus TACC3 RNAi suggest that the levels are indeed lower, arguing for the second possibility. Whatever the reason, we think that it is possible that RNAi phenotypes of other spindle proteins may

Fig. 8. TACC3 KS at metaphase alters kinetochore dynamics and decreases spindle length. Analysis of kinetochore motions in live HeLa cells stably expressing CENP-A-GFP and Centrin-GFP. Cells were depleted of endogenous TACC3 and were coexpressing PAGFP-MitoTrap and either mCherry-TACC3 or mCherry-FKBP-TACC3 and were treated with DMSO (vehicle) or rapamycin (200 nM). (**A–C**) Three example kinetochore trajectories from typical cells are shown. Left: Images of automated kinetochore tracking. Right: Plots of kinetochore distances relative to the metaphase plate as a function of time. Tracks of two sisters are shown for each pair; difference plot is shown (dotted line). (**D**) Diagram to show the measurement of d and x. (**E**) Population data for sister separation (d, inter-kinetochore distance) and sister center normal position (x). (**F**) Sister center normal displacement (Δx auto-correlation). Line thickness represents 95% confidence interval. Peaks of negative and positive lobes (half- and full-period) are shown by dashed and full vertical lines, respectively. (**G**) Mean squared displacement analysis for kinetochore pairs. Error bars show s.e.m. (**H**) Image to show the automated 4D tracking of spindle poles (centrin-GFP) in addition to kinetochores (see Materials and Methods). See supplementary material Movie 3. (**I**) Euclidian interpolar distances (S) for each condition. Color coding is the same as in previous figures. (**J**) Scatter plots to show that the average inter-kinetochore distance (d) does not vary as a function of spindle length (S). Insets show control data (above) and TACC3 KS data (below) for reference; a line of best fit is shown (r^2=0.08 and 0.11, respectively). Analysis in all figure panels is from four independent experiments.

have been similarly underestimated. Revisiting some of these proteins using KS in the future may give a more accurate picture of their mitotic function(s).

Materials and Methods

Molecular biology

To make pBrain-GFP-FKBP-TACC3KDP-shTACC3, an FKBP fragment was amplified from gamma-FKBP by PCR and inserted into pBrain-GFP-TACC3KDP-shTACC3 via Acc65I/BsrGI and Acc65I. To make mCherry- or PAGFP-MitoTrap, YFP in YFP-MitoTrap (pMito-YFP-FRB) was replaced with either mCherry or photo-activatable-GFP (PAGFP) via AgeI and BsrGI. PAGFP-MitoTrap was used as an 'invisible' MitoTrap to make other channels available for experiments (Willox and Royle, 2012). Gamma-FKBP and YFP-MitoTrap were kind gifts from Prof. M. S. Robinson (Cambridge Institute for Medical Research, UK).

For clathrin rerouting experiments, GFP-FKBP-LCa was used with no RNAi. GFP-FKBP-LCa was made by inserting a PCR-amplified FKBP fragment between GFP and LCa via BsrGI/Acc65I. GFP was exchanged with mCherry to make mCherry-H2B using AgeI/NotI from GFP-H2B. GFP-H2B, GFP-LCa and pBrain-GFP-TACC3KDP-shTACC3 were available from previous work (Booth et al., 2011; Royle et al., 2005).

Cell culture, reagents and antibodies

HeLa cells were cultured in Dulbecco's Modified Eagle Medium (Invitrogen) supplemented with 10% fetal bovine serum (FBS) and 100 U/ml penicillin/streptomycin at 37℃ and 5% CO_2. Cells were transfected using GeneJuice (Novagen). Rapamycin (SigmaAldrich) was used at 200 nM, vehicle was ethanol (0.1%). MLN8237 (Selleck) was used at 1 μM, vehicle was DMSO (0.01%).

For indirect immunofluorescence, HeLa on coverslips were fixed with PTEMF (50 mM PIPES [1,4-Piperazinediethanesulfonic acid], pH 7.2, 10 mM EGTA, 1 mM $MgCl_2$, 0.2% Triton X-100, 4% paraformaldehyde) at room temperature, or methanol at −20℃ for ch-TOG staining. Cells were then permeabilized (PBS with 0.5% Triton X-100) and blocked (PBS with 5% BSA and 5% goat serum). The following antibodies were used: (1) mouse monoclonals: clathrin heavy chain (X22, CRL-2228 ATCC), TACC3 (ab56595, Abcam), and Eg5 (611186, BD Biosciences) (2) mouse polyclonal: GTSE1 (H00051512-B01P, Abnova), (3) rabbit polyclonals: ch-TOG (34032, Autogen Bioclear) and β-tubulin (ab6046, Abcam), NuMA (3888s, Cell Signaling), HURP (kind gift from Prof. E. A. Nigg, University of Basel, Switzerland), Mad2 (Covance), (4) human polyclonal: Crest (CS1058, Europa Bioproducts). Fluorescently-conjugated secondary antibodies were Alexa488, Alexa568 or Alexa633 (Molecular Probes). Coverslips were mounted using Mowiol containing 4′,6-diamidino-2-phenylindole (DAPI).

Light microscopy

Live-cell imaging of KS kinetics was performed on an Olympus IX71 in glass-bottom dishes heated to 37℃ (Bioptechs Delta T5 μ-environmental culture dish controller) in CO_2-independent medium (Invitrogen) supplemented with 10% FBS and 100 U/ml penicillin/streptomycin, using Cell-R acquisition software and a Hamamatsu ORCA-ER C4742-80 camera with a 60× oil-immersion objective (1.42 NA). Quantification of GFP intensity during KS was performed using ImageJ, with an ROI that defined the spindle and one that excluded it, and plotted as $\Delta F/F_0$.

Live-cell imaging of mitotic progression following RNAi or KS was performed on a Nikon Eclipse Ti with a heated Perspex chamber (OKOlab) using standard filter sets for visualization of GFP and mCherry, NIS acquisition software, a CoolSNAP HQ2 camera and a 20× air objective (0.45 NA). Cells were kept at 37℃, in supplemented CO_2-independent medium. Light intensity was kept to a minimum to avoid light-induced cell damage. Chromosomes were visualized with mCherry-H2B (imaged once per minute), and GFP monitored every 5 minutes. Rapamycin was added to 200 nM by adding a concentrated media solution at 37℃ to the cell culture medium. Note that, for rerouting at metaphase, KS was induced at a variable time after the last chromosome aligned. It is likely therefore that we have underestimated the metaphase delay.

Confocal imaging was performed using a Leica confocal microscope SP2 with a 63× (1.4 NA) oil-immersion objective as described previously (Booth et al., 2011). For inter-kinetochore distance measurements, Z-stacks of CREST-immunostained cells were taken, assembled in ImageJ and distances between unambiguous CREST-positive kinetochore pairs in the stack were measured. For measurement of TACC3 levels, fixed, stained cells were imaged using identical acquisition parameters for all conditions. Mean pixel intensity for TACC3 was measured in a 20×20 pixel ROI using ImageJ software and the background subtracted.

Epifluorescence images of fixed cells were taken using a Nikon Eclipse Ti-U microscope with standard filter sets for visualization of DAPI, GFP, Alexa Fluor 568 and Alexa Fluor 633, a Nikon Digital Sight DS-Qi1Mc camera, a 60× (1.40 NA) oil-immersion objective and NIS acquisition software. To quantify Mad2 recruitment to the kinetochore, cells immunostained for Mad2 and CREST were imaged throughout the full Z dimension of the metaphase plate, and Mad2 puncta which colocalized with CREST were counted.

Cold-stable MT assay and analysis was performed as described previously (Toso et al., 2009). Briefly, cells treated with RNAi (48 hours) or KS (30 minutes), were placed in ice-cold medium, and incubated on ice for 10 minutes. The cells were then fixed with PTEMF and stained for tubulin and CREST. Confocal Z stacks were taken of metaphase cells and analyzed using Imaris as described.

4D kinetochore and spindle pole tracking

Cells were seeded in 35-mm Fluorodishes (WPI) in DMEM with 10% FBS and imaged on a widefield imaging system (Personal DeltaVision; Applied Precision) fitted with an environmental chamber maintained at 37℃ and 10% CO_2 atmospheric concentration. Images were acquired with a 100× 1.35 NA objective (Olympus) and a CDC (CoolSnap HQ2; Photometrics). Image acquisition was controlled by the softWoRx software suite (Applied Precision), 15 image stacks spaced 0.5 μm apart were collected every 7.5 seconds for 5 minutes (41 time-points). Pixels were set to 1×1 binning (65 nm effective pixel size).

Movies were deconvolved in softWoRx before tracking analysis. Automatic kinetochore tracking was performed as described (Jaqaman et al., 2010). All analysis was performed in MATLAB R2012a (MathWorks) with core algorithms written in C (compiled with the MATLAB MEX compiler). Only inlier kinetochores were used for analysis (spots that were $<2.5\sigma$ from metaphase plate).

Spindle pole tracks were identified by assigning a cost to each pair of tracks. The cost was defined as $c=|d-s| * a$ where d was the average distance between the tracks, s was the expected average spindle length, set to 11 μm and a was the average angle between the tracks and the metaphase plate. Tracks were only considered if $d>5$ μm and $a<30^{\circ}$, and if both tracks were unaligned throughout both their lifetimes. The pair of tracks with the lowest cost was chosen. Since both centrioles in each pole were tagged, the second centriole track for each pole was found by assigning a cost: $c=g^{-1}$ where g was the cross-correlation between the pole track and the candidate track. Tracks were only considered if $g>0.9$ and if the average distance between the tracks was less than 1 μm. The track with the lowest cost was chosen for each pole as its respective second centriole.

For pole tracks where two centrioles were found, the pole position was defined as the center point between the two, otherwise the position of a single centriole was used. Spindle length was taken as the 3D distance between the two poles.

Correlative light-electron microscopy

Correlative light-electron microscopy was performed as previously (Booth et al., 2011). HeLa cells were transfected with mCherry-MitoTrap and either pBrain-GFP-FKBP-TACC3KDP-shTACC3 or pBrain-GFP-TACC3KDP-shTACC3. Tomograms were assembled from tilt image series using eTOMO software (Boulder Laboratory for 3D Electron Microscopy). Quantification of EM images was carried out by an experimenter blind to the conditions of the experiment. All methods were as described previously (Booth et al., 2011), with the following exceptions. MT positions and cross-sectional area were plotted and calculated in tomograms. For measurement of K-fiber cross-sectional area, a 40 nm perimeter was computed around clusters of annotated MTs and measured using ImageJ. MTs within this boundary were counted as part of the K-fiber. To measure inter-MT distances, a map of MTs was created using IMOD Software (Boulder Laboratory for 3D Electron Microscopy), the coordinates were exported using model2point. The distance between each point was calculated in Microsoft Excel, from here the distance for each MT and its nearest neighboring MT was selected. To give the edge-to-edge distance, 20 nm was subtracted from these measurements. Neighbor density analysis was performed using nda in IMOD. MTs were annotated as circles of ~25 nm diameter throughout the Z slices, and flattened to a single Z plane. MTs within 80 nm of each other were padded by 50 nm using a convex polygon boundary.

Data analysis

Statistical testing was performed with InStat or SPSS. Normally distributed data were compared using one-way ANOVA followed by a Tukey–Kramer *post hoc* test. Student's unpaired *t*-test was used to compare two data sets. Non-parametric data were compared using Kruskal–Wallis' ANOVA test. The Kolmogorov–Smirnov test was used to determine if the data followed a Gaussian distribution. Cox regression analysis was used to test for significance of mitotic delays. Tukey box plots show the median, interquartile range and the 10th and 90th percentile. Figures were assembled using IgorPro 6.22A (Wavemetrics), Matlab (R2012), Adobe Photoshop and Adobe Illustrator.

Acknowledgements

We thank members of the Royle laboratory for useful comments and Sylvie Urbé for generous access to her live-cell imaging system. We are grateful to Scottie Robinson and Erich Nigg for essential reagents and David Mastronarde for advice and help with nda/IMOD. The authors declare that they have no conflict of interest.

Author contributions

L.P.C. designed, carried out and analyzed the experiments, E.F.H. and A.D.M. helped with tracking experiments and analysis, I.A.P. helped with the design and implementation of electron microscopy, S.J.R. designed the experiments, analyzed data, coordinated the work and wrote the manuscript with input from all authors.

Funding

L.P.C. is the recipient of a Wellcome Trust Prize Studentship. This work was supported by a Career Establishment Award from Cancer Research UK [grant number C25425/A8722 to S.J.R.]. S.J.R. is a Senior Cancer Research Fellow for Cancer Research UK. A.D.M. was supported by a Biotechnology and Biological Sciences Research Council (BBSRC) project grant [grant number BB/I021353/1]. E.F.H. was supported by the Engineering and Physical Sciences Research Council (EPSRC) [grant number EP/F500378/1] via the MOAC doctoral training centre. Deposited in PMC for release after 6 months.

Supplementary material available online at
http://jcs.biologists.org/lookup/suppl/doi:10.1242/jcs.124834/-/DC1

References

Barr, A. R. and Gergely, F. (2008). MCAK-independent functions of ch-Tog/XMAP215 in microtubule plus-end dynamics. *Mol. Cell. Biol.* **28**, 7199-7211.

Booth, D. G., Hood, F. E., Prior, I. A. and Royle, S. J. (2011). A TACC3/ch-TOG/clathrin complex stabilises kinetochore fibres by inter-microtubule bridging. *EMBO J.* **30**, 906-919.

Borner, G. H., Antrobus, R., Hirst, J., Bhumbra, G. S., Kozik, P., Jackson, L. P., Sahlender, D. A. and Robinson, M. S. (2012). Multivariate proteomic profiling identifies novel accessory proteins of coated vesicles. *J. Cell Biol.* **197**, 141-160.

Brodsky, F. M. (2012). Diversity of clathrin function: new tricks for an old protein. *Annu. Rev. Cell Dev. Biol.* **28**, 309-336.

Cassimeris, L., Becker, B. and Carney, B. (2009). TOGp regulates microtubule assembly and density during mitosis and contributes to chromosome directional instability. *Cell Motil. Cytoskeleton* **66**, 535-545.

Charlebois, B. D., Kollu, S., Schek, H. T., Compton, D. A. and Hunt, A. J. (2011). Spindle pole mechanics studied in mitotic asters: dynamic distribution of spindle forces through compliant linkages. *Biophys. J.* **100**, 1756-1764.

Cheeseman, L. P., Booth, D. G., Hood, F. E., Prior, I. A. and Royle, S. J. (2011). Aurora A kinase activity is required for localization of TACC3/ch-TOG/clathrin inter-microtubule bridges. *Commun. Integr. Biol.* **4**, 409-412.

Dumont, S. and Mitchison, T. J. (2009). Compression regulates mitotic spindle length by a mechanochemical switch at the poles. *Curr. Biol.* **19**, 1086-1095.

Fu, W., Tao, W., Zheng, P., Fu, J., Bian, M., Jiang, Q., Clarke, P. R. and Zhang, C. (2010). Clathrin recruits phosphorylated TACC3 to spindle poles for bipolar spindle assembly and chromosome alignment. *J. Cell Sci.* **123**, 3645-3651.

Fu, W., Jiang, Q. and Zhang, C. (2011). Novel functions of endocytic player clathrin in mitosis. *Cell Res.* **21**, 1655-1661.

Gergely, F., Karlsson, C., Still, I., Cowell, J., Kilmartin, J. and Raff, J. W. (2000a). The TACC domain identifies a family of centrosomal proteins that can interact with microtubules. *Proc. Natl. Acad. Sci. USA* **97**, 14352-14357.

Gergely, F., Kidd, D., Jeffers, K., Wakefield, J. G. and Raff, J. W. (2000b). D-TACC: a novel centrosomal protein required for normal spindle function in the early Drosophila embryo. *EMBO J.* **19**, 241-252.

Gergely, F., Draviam, V. M. and Raff, J. W. (2003). The ch-TOG/XMAP215 protein is essential for spindle pole organization in human somatic cells. *Genes Dev.* **17**, 336-341.

Giet, R., Uzbekov, R., Cubizolles, F., Le Guellec, K. and Prigent, C. (1999). The Xenopus laevis aurora-related protein kinase pEg2 associates with and phosphorylates the kinesin-related protein XlEg5. *J. Biol. Chem.* **274**, 15005-15013.

Hepler, P. K., McIntosh, J. R. and Cleland, S. (1970). Intermicrotubule bridges in mitotic spindle apparatus. *J. Cell Biol.* **45**, 438-444.

Hirst, J., Borner, G. H., Antrobus, R., Peden, A. A., Hodson, N. A., Sahlender, D. A. and Robinson, M. S. (2012). Distinct and overlapping roles for AP-1 and GGAs revealed by the 'knocksideways' system. *Curr. Biol.* **22**, 1711-1716.

Hubner, N. C., Bird, A. W., Cox, J., Splettstoesser, B., Bandilla, P., Poser, I., Hyman, A. and Mann, M. (2010). Quantitative proteomics combined with BAC TransgeneOmics reveals in vivo protein interactions. *J. Cell Biol.* **189**, 739-754.

Jaqaman, K., King, E. M., Amaro, A. C., Winter, J. R., Dorn, J. F., Elliott, H. L., McHedlishvili, N., McClelland, S. E., Porter, I. M., Posch, M. et al. (2010). Kinetochore alignment within the metaphase plate is regulated by centromere stiffness and microtubule depolymerases. *J. Cell Biol.* **188**, 665-679.

Kettenbach, A. N., Schweppe, D. K., Faherty, B. K., Pechenick, D., Pletnev, A. A. and Gerber, S. A. (2011). Quantitative phosphoproteomics identifies substrates and functional modules of Aurora and Polo-like kinase activities in mitotic cells. *Sci. Signal.* **4**, rs5.

Khodjakov, A. and Pines, J. (2010). Centromere tension: a divisive issue. *Nat. Cell Biol.* **12**, 919-923.

Kinoshita, K., Noetzel, T. L., Pelletier, L., Mechtler, K., Drechsel, D. N., Schwager, A., Lee, M., Raff, J. W. and Hyman, A. A. (2005). Aurora A phosphorylation of TACC3/maskin is required for centrosome-dependent microtubule assembly in mitosis. *J. Cell Biol.* **170**, 1047-1055.

Lee, M. J., Gergely, F., Jeffers, K., Peak-Chew, S. Y. and Raff, J. W. (2001). Msps/XMAP215 interacts with the centrosomal protein D-TACC to regulate microtubule behaviour. *Nat. Cell Biol.* **3**, 643-649.

Lin, C. H., Hu, C. K. and Shih, H. M. (2010). Clathrin heavy chain mediates TACC3 targeting to mitotic spindles to ensure spindle stability. *J. Cell Biol.* **189**, 1097-1105.

McDonald, K. L., O'Toole, E. T., Mastronarde, D. N. and McIntosh, J. R. (1992). Kinetochore microtubules in PTK cells. *J. Cell Biol.* **118**, 369-383.

McEwen, B. F., Heagle, A. B., Cassels, G. O., Buttle, K. F. and Rieder, C. L. (1997). Kinetochore fiber maturation in PtK1 cells and its implications for the mechanisms of chromosome congression and anaphase onset. *J. Cell Biol.* **137**, 1567-1580.

Murray, A. W. (2011). A brief history of error. *Nat. Cell Biol.* **13**, 1178-1182.

Nicklas, R. B., Kubai, D. F. and Hays, T. S. (1982). Spindle microtubules and their mechanical associations after micromanipulation in anaphase. *J. Cell Biol.* **95**, 91-104.

Nishimura, K., Fukagawa, T., Takisawa, H., Kakimoto, T. and Kanemaki, M. (2009). An auxin-based degron system for the rapid depletion of proteins in nonplant cells. *Nat. Methods* **6**, 917-922.

Peset, I. and Vernos, I. (2008). The TACC proteins: TACC-ling microtubule dynamics and centrosome function. *Trends Cell Biol.* **18**, 379-388.

Peterman, E. J. and Scholey, J. M. (2009). Mitotic microtubule crosslinkers: insights from mechanistic studies. *Curr. Biol.* **19**, R1089-R1094.

Piekorz, R. P., Hoffmeyer, A., Duntsch, C. D., McKay, C., Nakajima, H., Sexl, V., Snyder, L., Rehg, J. and Ihle, J. N. (2002). The centrosomal protein TACC3 is essential for hematopoietic stem cell function and genetically interfaces with p53-regulated apoptosis. *EMBO J.* **21**, 653-664.

Robinson, M. S., Sahlender, D. A. and Foster, S. D. (2010). Rapid inactivation of proteins by rapamycin-induced rerouting to mitochondria. *Dev. Cell* **18**, 324-331.

Royle, S. J. (2011). Mitotic moonlighting functions for membrane trafficking proteins. *Traffic* **12**, 791-798.

Royle, S. J. (2012). The role of clathrin in mitotic spindle organisation. *J. Cell Sci.* **125**, 19-28.

Royle, S. J., Bright, N. A. and Lagnado, L. (2005). Clathrin is required for the function of the mitotic spindle. *Nature* **434**, 1152-1157.

Schneider, L., Essmann, F., Kletke, A., Rio, P., Hanenberg, H., Wetzel, W., Schulze-Osthoff, K., Nürnberg, B. and Piekorz, R. P. (2007). The transforming acidic coiled coil 3 protein is essential for spindle-dependent chromosome alignment and mitotic survival. *J. Biol. Chem.* **282**, 29273-29283.

Toso, A., Winter, J. R., Garrod, A. J., Amaro, A. C., Meraldi, P. and McAinsh, A. D. (2009). Kinetochore-generated pushing forces separate centrosomes during bipolar spindle assembly. *J. Cell Biol.* **184**, 365-372.

Waters, J. C., Chen, R. H., Murray, A. W. and Salmon, E. D. (1998). Localization of Mad2 to kinetochores depends on microtubule attachment, not tension. *J. Cell Biol.* **141**, 1181-1191.

Willox, A. K. and Royle, S. J. (2012). Stonin 2 is a major adaptor protein for clathrin-mediated synaptic vesicle retrieval. *Curr. Biol.* **22**, 1435-1439.

Yu, C. T., Hsu, J. M., Lee, Y. C., Tsou, A. P., Chou, C. K. and Huang, C. Y. (2005). Phosphorylation and stabilization of HURP by Aurora-A: implication of HURP as a transforming target of Aurora-A. *Mol. Cell. Biol.* **25**, 5789-5800.